Citation
Hingee, K. and Baddeley, A. and Caccetta, P. and Nair, G. 2019. Computation of Lacunarity from Covariance of Spatial Binary Maps. Journal of Agricultural, Biological, and Environmental Statistics. 24 (2): pp. 264-288. http://doi.org/10.1007/s13253-019-00351-9

Computation of lacunarity from covariance of spatial binary maps

October 5, 2018

Abstract

We consider a spatial binary coverage map (binary pixel image) which might represent the spatial pattern of presence and absence of vegetation in a landscape. "Lacunarity" is a generic term for the nature of gaps in the pattern: a popular choice of summary statistic is the "gliding box lacunarity" curve (GBL). GBL is potentially useful for quantifying changes in vegetation patterns, but its application is hampered by difficulties with missing data. In this paper we find a mathematical relationship between GBL and spatial covariance. This leads to new estimators of GBL that tolerate irregular spatial domains and missing data, thus overcoming major weaknesses of the traditional estimator. The relationship gives an explicit formula for GBL of models with known spatial covariance and enables us to predict the effect on GBL of changes in the pattern. Using variance reduction methods for spatial data, we obtain statistically efficient estimators of GBL. The techniques are demonstrated on simulated binary coverage maps, and remotely-sensed maps of local-scale disturbance and meso-scale fragmentation in Australian forests. Results show in some cases a four-fold reduction in mean integrated squared error and a twenty-fold reduction in sensitivity to missing data. Online supplementary material includes additional detail and a software implementation in the R language.

Key Words: forest disturbance; fractal; gliding box; image analysis; random set; spatial statistics.

1 Introduction

Figure 1 is a spatial binary coverage map, a binary-valued pixel image showing the presence and absence of vegetation in a study region (Diggle, 1981). Statistical analysis of spatial coverage maps have important applications in biology, ecology, geography, food science, materials science and other fields (Serra, 1982; Stoyan and Stoyan, 1994; Chiu et al., 2013).

[Figure 1 about here.]

Lacunarity is a generic term for 'the nature of gaps' in the pattern (Mandelbrot, 1983, §34). One popular choice of summary statistic for lacunarity is the *gliding box lacunarity* (GBL) curve introduced by Allain and Cloitre (1991) and popularised by Plotnick et al. (1993, 1996). For two-dimensional spatial patterns $\mathbb{X}$ with positive coverage fraction, such as Figure 1, the GBL index is

$$\mathrm{L}(B) := \frac{\mathbb{E}\big[|\mathbb{X} \cap B|^2\big]}{\mathbb{E}\left[|\mathbb{X} \cap B|\right]^2} = \frac{\mathrm{Var}\big(|\mathbb{X} \cap B|\big)}{\mathbb{E}\left[|\mathbb{X} \cap B|\right]^2} + 1, \tag{1}$$

where B is a test set of given shape and size, and $|\cdot|$ denotes the area of a set. Typically B is chosen to be a square of side length s, and the index $L(B)$ is plotted as a function of s. The expectation and variance in (1) are averages over possible outcomes of the random spatial pattern $\mathbb{X}$, or equivalently, averages over random positions of B relative to an observed pattern $\mathbb{X}$, as explained in Section 2.2.

GBL has been applied to soil moisture (Cumbrera et al., 2012), radar echos (Azzaz and Haddad, 2017), urban land cover (Myint and Lam, 2005), ham quality (Valous et al., 2009), ecosystem services (Roces-Díaz et al., 2014), landscape evapotranspiration (Liu and Zhang, 2010), deforestation (Pintilii et al., 2017), urbanisation (Sung et al., 2013), racial segregation (Sui and Wu, 2006), biological tissues (Gould et al., 2011; Shah et al., 2016), and crystallisation (Velazquez-Camilo et al., 2010).

A major limitation of all existing techniques for GBL is the difficulty of applying them when the observation window W is not a rectangle (Sui and Wu, 2006) or when data are missing for some pixels. In order for the intersection area $|\mathbb{X} \cap B|$ to be measured, the test set B must lie entirely inside the region W where $\mathbb{X}$ is observed. The gliding-box algorithm of Allain and Cloitre (1991) involves placing a translated copy of B at every possible position inside W. If W is not a rectangle, valid positions of B may be rare or nonexistent, so that $L(B)$ cannot be computed reliably. However, observation windows with complicated geometry arise frequently. Administrative regions, property ownership, mining leases, and land management areas are demarcated by irregular polygonal boundaries. Irregular shapes are typical of human settlements (Owen and University, 2011; Owen, 2012; Sui and Wu, 2006) and slices of physical materials and food. Observation windows may have holes caused by natural phenomena such as lakes, fire scars in forests, mineral inclusions in rocks, and blood vessels in histological sections. Data may be missing because of pixel noise, specular reflections, preparation artefacts in microscopy, or cloud occlusions in satellite images. This problem is widely recognised; proposed solutions include reconstruction of missing data (Shah et al., 2016).

In this paper we derive a mathematical relation between GBL and spatial covariance, for random sets with positive coverage fraction. This relation leads to new estimators of GBL that tolerate extremely complicated observation windows and missing data, thus overcoming a major weaknesses of the traditional gliding-box estimator. The relation also provides insight into the behaviour of GBL, and assists with interpreting GBL estimates. For some spatial models, the relation provides explicit expressions for GBL as a function of model parameters. Using variance reduction ideas (Picka, 2000), we develop statistically efficient estimators of GBL. The differences between our estimators and the traditional gliding-box estimator are due to different treatment of data near the edges of the observation window, suggesting that our methods, regardless of the particular model assumptions, summarise binary maps in the same way as the traditional estimator. We demonstrate our estimators on simulated binary maps; on a time-series of forest maps derived from Landsat satellite images that contain clouds and missing data; and on decimetre-resolution tree canopy maps of fragmented forest parcels.

There are at least seven other indices of lacunarity available in the literature (surveyed in Section 2.3 below). While many of these alternative indices are superficially similar to GBL, they do not have a direct relationship to the spatial covariance, and therefore do not enjoy the benefits described above.

The plan of the paper is as follows. In Section 2 we state essential background on random sets, give formal definitions of spatial covariance and GBL, and survey other lacunarity indices in the literature. In Section 3 we establish that GBL is a function of the spatial covariance, and explore its properties. In Section 4 we define new covariance-based estimators of GBL and investigate their mathematical relationship to the gliding box estimator. In Sections 5 and 6 we apply our estimators to simulated binary maps and forest maps, respectively. The online supplementary material includes estimates of the computational cost of the estimators, further details relevant to Sections 2–6, and a software implementation in the R language.

2 Background

2.1 Random Closed Sets

A *random closed set* (RACS) $\mathbb{X}$ in $\mathbb{R}^d$ is a random element of the set of closed subsets of $\mathbb{R}^d$ such that the probability of $\mathbb{X}$ intersecting any given compact subset of $\mathbb{R}^d$ is well defined. For formal definitions of RACS and their properties, see Matheron (1975), Molchanov (2005) or Chiu et al. (2013). The probability distribution of a RACS $\mathbb{X}$ is completely determined by its capacity functional $T_{\mathbb{X}}(K) = P(\mathbb{X} \cap K \neq \varnothing)$ defined for all compact subsets K of $\mathbb{R}^d$ (Molchanov, 2005).

2.1.1 Properties of RACS

The vector shift (translation) of a set $A \subseteq \mathbb{R}^d$ by a vector $\mathbf{v} \in \mathbb{R}^d$ is denoted

$$A \oplus \mathbf{v} = \{a + \mathbf{v} : \ a \in A\}.$$

A random closed set $\mathbb{X}$ is called *stationary* if, for every $\mathbf{v}$ in $\mathbb{R}^d$, the distribution of $\mathbb{X} \oplus \mathbf{v}$ is the same as the distribution of $\mathbb{X}$. Stationary RACS are flexible models; a single realisation of a stationary RACS can appear complex and spatially irregular.

For a stationary RACS $\mathbb{X}$, the *coverage probability*

$$p := P(\mathbf{x} \in \mathbb{X}) \tag{2}$$

does not depend on the choice of the point $\mathbf{x} \in \mathbb{R}^d$. Likewise the *spatial covariance function* $C(\mathbf{v})$ of a stationary random closed set $\mathbb{X}$ in $\mathbb{R}^d$ is defined (Serra, 1982, §9) as the probability that two given points, separated by a vector $\mathbf{v}$, will both lie inside $\mathbb{X}$:

$$C(\mathbf{v}) := P(\mathbf{x} \in \mathbb{X}, \mathbf{x} + \mathbf{v} \in \mathbb{X}), \qquad \mathbf{x}, \mathbf{v} \in \mathbb{R}^d, \tag{3}$$

where this probability does not depend on $\mathbf{x}$. Note that $C(o) = p$, where o is the origin of $\mathbb{R}^d$. The spatial covariance function, also known as the *two-point phase probability* (Quintanilla, 2008), is closely related to the semivariogram of a random field (Serra, 1982, p280). Spatial covariance has been applied to numerous phenomena (Kautz et al., 2011; Nott and Wilson, 2000; Quintanilla et al., 2007; Serra, 1982), including the heather pattern in Figure 1 (Diggle, 1981). It is fundamental to determining macroscale properties of two-phase random media from microscale properties (Quintanilla, 2008) and can sometimes be computed from model parameters (Nott and Wilson, 2000; Chiu et al., 2013; Quintanilla, 2008). Interpretation, estimation and applications of covariance of RACS are discussed in detail by Serra (1982, §9).

Second-order moment properties of RACS closely related to covariance are the centred covariance $\kappa(\mathbf{v}) := C(\mathbf{v}) - p^2$ and the pair correlation function, $g(\mathbf{v}) := C(\mathbf{v})/p^2$. In Section 4 we will use estimators for covariance, pair correlation and centred covariance to define new estimators of GBL.

It is often reasonable to assume that a stationary RACS is *mixing* in the sense that

$$\lim_{|\mathbf{v}| \longrightarrow \infty} P(\mathbb{X} \cap (A \cup (B \oplus \mathbf{v})) = \varnothing) = P(\mathbb{X} \cap A = \varnothing) P(\mathbb{X} \cap B = \varnothing) \tag{4}$$

for any two compact subsets, A and B, of $\mathbb{R}^d$, where $\mathbf{v} \in \mathbb{R}^d$, and $|\mathbf{v}|$ is the length of $\mathbf{v}$ (Schneider and Weil, 2008, §9). Loosely speaking the mixing property is a sufficient condition for spatial averages over increasingly large observation windows to converge almost surely to their corresponding statistical moments (Chiu et al., 2013, §6.1.4).

2.1.2 Estimators of RACS Properties

For a set A in $\mathbb{R}^d$ we will call the d-dimensional volume of A, which is the area of A in $\mathbb{R}^2$ and the (usual) volume of A in $\mathbb{R}^3$, the *volume* of A, denoted by $|A|$. We will also use $\breve{A} = \{-\mathbf{a} : \mathbf{a} \in A\}$ to denote the reflection of A in the origin and $\mathbf{1}_A$ to denote the indicator function of A, defined as $\mathbf{1}_A(\mathbf{y}) = 1$, if $\mathbf{y}$ is in A, and $\mathbf{1}_A(\mathbf{y}) = 0$, otherwise.

The *set covariance* of a set A is defined as the volume of A intersected with a translated copy of A,

$$\gamma_A(\mathbf{v}) := |A \cap (A \oplus \mathbf{v})| = \int_{\mathbb{R}^d} \mathbf{1}_A(\mathbf{y}) \mathbf{1}_A(\mathbf{y} - \mathbf{v}) \, \mathrm{d}\mathbf{y}, \tag{5}$$

where $\mathbf{v} \in \mathbb{R}^d$ is the translation vector. The set covariance, $\gamma_A(\mathbf{v})$, can be computed quickly using the Fast Fourier Transform as the right-hand side of (5) is the convolution of $\mathbf{1}_A$ with $\mathbf{1}_{\breve{A}}$. In many ways set covariance is the analogue of $C(\mathbf{v})$ for deterministic sets (Serra, 1982, p272).

For a binary map with observation window W we consider the foreground to be $X \cap W$ where X is a realisation of a stationary RACS $\mathbb{X}$. Pixellation effects are ignored. The traditional estimators of p and $C(\mathbf{v})$ from such a binary map observation are (Chiu et al., 2013, §6.4.2, §6.4.3)

$$\hat{p} = \frac{|X \cap W|}{|W|} \tag{6}$$

$$\hat{C}(\mathbf{v}) = \frac{|X \cap W \cap ((X \cap W) \oplus \mathbf{v})|}{|W \cap (W \oplus \mathbf{v})|} = \frac{\gamma_{X \cap W}(\mathbf{v})}{\gamma_W(\mathbf{v})}. \tag{7}$$

The numerator of $\hat{C}(\mathbf{v})$ is the volume of the set of points $\mathbf{x}$ such that both $\mathbf{x}$ and $\mathbf{x} + \mathbf{v}$ are observed to lie in X, whilst the denominator is the volume of the set of points $\mathbf{w}$ for which both $\mathbf{w}$ and $\mathbf{w} + \mathbf{v}$ lie in the observation window. Since the numerator and denominator of (7) are set covariance functions, $\hat{C}(\mathbf{v})$ can be computed quickly using the Fast Fourier Transform (Koch et al., 2003).

Picka (1997, 2000) proposed 'balanced' estimators of centred covariance and pair correlation that have smaller variance than the traditional estimators, $\hat{\kappa}_T(\mathbf{v}) := \hat{C}(\mathbf{v}) - \hat{p}^2$

and $\hat{g}_T(\mathbf{v}) := \hat{C}(\mathbf{v})\,/\hat{p}^2$, respectively. If we define

$$\hat{p}_R(\mathbf{v}) := \frac{|X \cap W \cap (W \oplus \mathbf{v})|}{\gamma_W(\mathbf{v})} \quad \text{and} \quad \hat{H}(\mathbf{v}) := \hat{p}(\hat{p}_R(\mathbf{v}) + \hat{p}_R(-\mathbf{v}) - 2\hat{p}), \tag{8}$$

where $\hat{p}_R(\mathbf{v})$ is an unbiased coverage probability estimator of $\mathbb{X}$ that depends only on the binary map within $W \cap (W \oplus \mathbf{v})$, then the 'additively balanced' estimators of $\kappa(\mathbf{v})$ and $g(\mathbf{v})$ proposed by Picka are

$$\hat{\kappa}_H(\mathbf{v}) := \hat{C}(\mathbf{v}) - \hat{H}(\mathbf{v}) - \hat{p}^2 \qquad \text{and} \qquad \hat{g}_H(\mathbf{v}) := \frac{\hat{C}(\mathbf{v}) - \hat{H}(\mathbf{v})}{\hat{p}^2}, \tag{9}$$

respectively. Picka also proposed 'intrinsically balanced' estimators,

$$\hat{\kappa}_I(\mathbf{v}) := \hat{C}(\mathbf{v}) - \hat{p}_R(\mathbf{v})\,\hat{p}_R(-\mathbf{v}) \tag{10}$$

$$\hat{g}_I(\mathbf{v}) := \frac{\hat{C}(\mathbf{v})}{\hat{p}_R(\mathbf{v})\,\hat{p}_R(-\mathbf{v})} \tag{11}$$

$$\hat{g}_M(\mathbf{v}) := \frac{\hat{C}(\mathbf{v})}{\left(\frac{1}{2}(\hat{p}_R(\mathbf{v}) + \hat{p}_R(-\mathbf{v}))\right)^2}, \tag{12}$$

asserting that $\hat{g}_M(\mathbf{v})$ has larger variance than $\hat{g}_H(\mathbf{v})$ and $\hat{g}_I(\mathbf{v})$. Later Mattfeldt and Stoyan (2000) studied an isotropic estimator similar to $\hat{g}_M(\mathbf{v})$. The form of $\hat{g}_M(\mathbf{v})$ suggests to us another estimator of centred covariance,

$$\hat{\kappa}_M(\mathbf{v}) := \hat{C}(\mathbf{v}) - \left(\frac{1}{2}(\hat{p}_R(\mathbf{v}) + \hat{p}_R(-\mathbf{v}))\right)^2. \tag{13}$$

The additional computational costs of these balanced estimators over that of $\hat{C}(\mathbf{v})$ are not high, because the numerator of $\hat{p}_R(\mathbf{v})$ can be computed using the Fast Fourier Transform, and the denominator of $\hat{p}_R(\mathbf{v})$ is identical to that of $\hat{C}(\mathbf{v})$.

2.2 Gliding Box Lacunarity

GBL can be formally defined in two different ways, according to whether the binary map is assumed to be a fixed set or a random set (Allain and Cloitre, 1991). This duality is familiar in stochastic geometry (Chiu et al., 2013) and stereology (Baddeley and Jensen, 2005, Ch. 1). In this section we give definitions of GBL from both standpoints. The majority of the paper uses the random set standpoint, for convenience.

2.2.1 Fixed Set Scenario

Definition 1 *Suppose X is a set with positive volume within a bounded region of interest, Z, in $\mathbb{R}^d$. Given a compact set B, with $|B| > 0$, define the empirical* gliding box lacunarity *of X as*

$$\widehat{\mathrm{L}}_{GB}(B) := \frac{\mathrm{Var}\left(|X \cap \mathbf{B}|\right)}{\mathbb{E}\left[|X \cap \mathbf{B}|\right]^2} + 1 = \frac{\mathbb{E}\left[|X \cap \mathbf{B}|^2\right]}{\mathbb{E}\left[|X \cap \mathbf{B}|\right]^2}, \tag{14}$$

where $\mathbf{B} = B \oplus \mathbf{Y} \subseteq Z$ denotes a randomly translated copy of B by a random vector $\mathbf{Y}$ uniformly distributed in the set of feasible vectors

$$Z \ominus \check{B} = \{\mathbf{y} : B \oplus \mathbf{y} \subseteq Z\}.$$

termed the erosion *of Z by B. If the erosion has zero volume, GBL is undefined.*

Typically B is termed a 'box' and is often a square, although Allain and Cloitre noted that any shape is permitted. We have used a 'hat' here as we will see later (Section 2.2.2) to indicate that this version of GBL is an estimator of the random set GBL.

The first and second moment on the right hand side of (14) can be decomposed as

$$\mathbb{E}\left[|X \cap \mathbf{B}|\right] = \frac{1}{|Z \ominus \check{B}|} \int_{Z \ominus \check{B}} |X \cap (B \oplus \mathbf{y})| \,\mathrm{d}\mathbf{y} \tag{15}$$

$$\mathbb{E}\left[|X \cap \mathbf{B}|^2\right] = \frac{1}{|Z \ominus \check{B}|} \int_{Z \ominus \check{B}} |X \cap (B \oplus \mathbf{y})|^2 \,\mathrm{d}\mathbf{y}. \tag{16}$$

In practice, these integrals will be approximated by sums over a grid of pixels or sample points. The gliding box algorithm (Allain and Cloitre, 1991) computes (15) and (16) numerically using a fine lattice of box centres, $\mathbf{y}$, in $Z \ominus \check{B}$. The tug-of-war algorithm for lacunarity, proposed by Reiss et al. (2016), is a computationally efficient algorithm that approximates $\widehat{\mathrm{L}}_{\mathrm{GB}}(B)$. *Fixed-grid lacunarity* in the `frac2D` package (Reiss, 2016) is the exponent of a power-law approximation to estimates of $\widehat{\mathrm{L}}_{\mathrm{GB}}(B)$ that use non-overlapping box locations (Helmut Ahammer, personal communication 31 July 2018).

For raster binary maps, many authors use box widths ranging between 1 pixel wide and half the shortest side length of the binary map (Plotnick et al., 1993). It is also common to have shorter maximum box widths, or to use boxes equal to the extent of the binary map (Roces-Díaz et al., 2014; McIntyre and Wiens, 2000; Valous et al., 2009; Gould et al., 2011; Reiss et al., 2016).

Observation Window Difficulties In applications it is often the case that the region of interest, Z, is replaced by the observation window, W. However, using $W = Z$ leads to unequal treatment of data, as some locations close to the boundary of W are less likely to be inside $\mathbf{B}$ than locations in the interior of W, and some locations in W may have zero probability of being in $\mathbf{B}$. When the observation window geometry is complicated, especially when this is caused by sporadically missing data, or when B is large relative to the observation window, there are very few available locations for $\mathbf{B}$, and this unequal treatment of data can have a large impact on $\widehat{\mathrm{L}}_{\mathrm{GB}}(B)$. Modifications to $\widehat{\mathrm{L}}_{\mathrm{GB}}$ to solve this problem for rectangular observation windows and a limited class of observation windows were proposed by Feagin et al. (2007) and Sui and Wu (2006), respectively.

2.2.2 Random Set Scenario

Definition 2 *Suppose $\mathbb{X}$ is a stationary RACS in $\mathbb{R}^d$ with a positive coverage probability and B is a fixed compact set with positive volume. Define the GBL of $\mathbb{X}$ given B as*

$$\mathrm{L}(B) := \frac{\mathrm{Var}\left(|\mathbb{X} \cap B|\right)}{\mathbb{E}\left[|\mathbb{X} \cap B|\right]^2} + 1 = \frac{\mathbb{E}\left[|\mathbb{X} \cap B|^2\right]}{\mathbb{E}\left[|\mathbb{X} \cap B|\right]^2}, \tag{17}$$

where $|\mathbb{X} \cap B|$ is the volume of $\mathbb{X}$ within B.

The above definition is analogous to that of fixed-set GBL, with random translations of X instead of random translations of the box B as $|X \cap \mathbf{B}|$ can be written $|X \cap \mathbf{B}| = |(X \oplus -\mathbf{Y}) \cap B|$. The fixed set GBL definition is not quite redundant here as $\mathbf{Y}$ is such that $\mathbf{B}$ is always inside the region of interest Z and so $\mathbb{X} = X \oplus -\mathbf{Y}$ is not stationary in $\mathbb{R}^d$.

$\widehat{\mathrm{L}}_{\mathbf{GB}}(B)$ **as an Estimator of** $\mathrm{L}(B)$ If X is a realisation of a stationary and mixing RACS $\mathbb{X}$, then the spatial averages (15) and (16) over increasingly large regions of interest, Z, converge almost surely to their theoretical expectations $\mathbb{E}\left[|\mathbb{X} \cap B|\right]$ and $\mathbb{E}\left[|\mathbb{X} \cap B|^2\right]$, respectively. Thus $\widehat{\mathrm{L}}_{\mathrm{GB}}(B)$ converges to $\mathrm{L}(B)$ almost surely and $\widehat{\mathrm{L}}_{\mathrm{GB}}(B)$ is a consistent estimator of $\mathrm{L}(B)$.

In this paper we adopt the random set scenario; however, our main contributions still hold if we had instead used the fixed set scenario. In Section 4 we prove that our new methods approximate the fixed-set GBL, and it follows that fixed set GBL is approximately a function of set covariance. The results of Sections 5 and 6 show that our new methods produce better approximations to fixed-set GBL than the traditional method when the region of interest is partially observed.

2.3 Other Lacunarity Indices

The definition of the lacunarity of a pattern as the 'nature of gaps' in the pattern (Mandelbrot, 1983, §34) allows many mathematically distinct quantitative indices of lacunarity. The two most popular of these are GBL (Section 2.2) and sandbox lacunarity (described below) (Baveye et al., 2008), and have been compared by Allain and Cloitre (1991) and Pendleton et al. (2005). In some cases lacunarity indices have been named 'the lacunarity' in the literature, leading to confusion (Baveye et al., 2008). Applications can depend crucially on the choice of the lacunarity index and we suggest that the term 'lacunarity' should not be used as if it were a single quantity.

Many lacunarity indices use the mass of a set of interest within user-defined test sets, where the precise meaning of *mass* depends on the set of interest and the test set, usually denoted B below, is typically either a square or a disc centred on the origin, o. For sets that are patterns of points, patterns of curves or have positive volume, the appropriate measure of mass is likely to be, respectively, the numbers of points, length or volume of the set of interest within the test set. For sets that are iteratively constructed fractals the mass at each step of the construction might also be used to compute a lacunarity index (Lin and Yang, 1986). Lacunarity indices for functions mapping $\mathbb{R}^2$ to $\mathbb{R}^1$ have also been proposed (Diaz et al., 2009; Dong, 2000; Myint and Lam, 2005).

In the following we summarise many existing lacunarity indices that appear to be suitable for describing sets with positive volume. We denote by $\mathbb{X}$ a stationary RACS with positive coverage probability and assume that the measure of mass is volume.

Initially Mandelbrot (1983, §34) appears to have suggested the lacunarity indices

$$\mathcal{L}_{M1}(B) := \frac{\operatorname{Var}\big(\,|B\cap\mathbb{X}|\,\big|\,|B\cap\mathbb{X}|>0\big)}{\mathbb{E}\big[\,|B\cap\mathbb{X}|\,\big|\,|B\cap\mathbb{X}|>0\big]^2} \quad \text{and} \quad \mathcal{L}_{M2}(B) := \frac{\mathbb{E}\left[|\mathbb{X}\cap B|\,\Big|\,o\in\mathbb{X}\right]}{\mathbb{E}[|\mathbb{X}\cap B|]}, \tag{18}$$

and a third index that may only be relevant to self-similar sets. We have demonstrated that $\mathcal{L}_{M1}$, defined in (18), is a combination of GBL and a spatial statistical contact distribution (Section C of the supplementary material). Later Mandelbrot and Stauffer (1994) proposed the index

$$\mathcal{L}_A(r,\theta) = \frac{\mathbb{E}\big[|\mathbb{X}\cap S||\mathbb{X}\cap\check{S}|\big|o\in\mathbb{X}\big] - \mathbb{E}\big[|\mathbb{X}\cap S|\big|o\in\mathbb{X}\big]\mathbb{E}\big[|\mathbb{X}\cap\check{S}|\big|o\in\mathbb{X}\big]}{\operatorname{Var}\big(|\mathbb{X}\cap S|\big|o\in\mathbb{X}\big)}, \tag{19}$$

where S is a given sector, with angular size θ, of a disc of radius r centred on the origin.

Sandbox lacunarity (Chappard et al., 2001), which resembles the index proposed by Voss (1986), can be interpreted as the average of

$$\mathcal{L}_S(B) := \frac{\operatorname{var}\left[|\mathbb{X}\cap B|\big|o\in\mathbb{X}\right]}{\mathbb{E}\left[|\mathbb{X}\cap B|\big|o\in\mathbb{X}\right]^2} \tag{20}$$

over a user-specified range of test set sizes. Borys et al. (2008) suggested an index that corresponds to

$$\mathcal{L}_B(B) := 1 + \frac{\operatorname{Var}\big(\,|B\cap\mathbb{X}|\,\big|\,|B|>|B\cap\mathbb{X}|>0\big)}{\mathbb{E}\big[\,|B\cap\mathbb{X}|\,\big|\,|B|>|B\cap\mathbb{X}|>0\big]^2} \tag{21}$$

in the random set scenario. The FracLac plugin appears to report estimates of $\mathrm{L}(B)$, $\mathcal{L}_{M1}(B)+1$, and two other lacunarity indices that use binned and reweighted distributions of box mass (Karperien, 2005, p13, §Lacunarity).

Applications of lacunarity indices beyond those already mentioned for GBL include description of the structure of protein gels (Dàvila and Parés, 2007) (appears to use $\mathcal{L}_{M1}$ - Section C of the supplementary material), the vacuole of lungs suffering from cancer (Borys et al., 2008), microglia (Karperien et al., 2013), urban settlements (Owen and University, 2011), biofilms (Anderson et al., 2015), porous rocks (Anovitz and Cole, 2015), coral reefs (Rankey, 2016), the effect of high-pressure treatments on rabbit sausage (Xue et al., 2017), orange juice cloudiness (Aghajanzadeh et al., 2017), and handwriting of patients taking antipsychotic drugs (Aznarte et al., 2014). Applications of lacunarity indices usually focus on differences given by different test set sizes (Mandelbrot, 1983; Plotnick et al., 1993), the average across a range of test set sizes (Chappard et al., 2001; Karperien, 2005), or the exponent of a power-law approximation of the lacunarity index (Allain and Cloitre, 1991; Cheng, 1997). Lacunarity indices appear to be popular for analysis of multiscale phenomena, perhaps due to the origins of lacunarity as a fractal analysis tool (Plotnick et al., 1996).

3 GBL as a Function of Covariance

The first key contribution of this paper is the following relation (22) between GBL and the covariance of a stationary RACS. We will prove the relation at the end of this section.

Theorem 1. *Suppose $\mathbb{X}$ is a stationary RACS in $\mathbb{R}^d$ with positive coverage probability and that B is a compact subset of $\mathbb{R}^d$ with positive volume. Then the GBL given by the 'box' B is equal to*

$$\mathrm{L}(B) = \frac{1}{p^2|B|^2} \int_{\mathbb{R}^d} \gamma_B(\mathbf{v}) C(\mathbf{v}) \, \mathrm{d}\mathbf{v}, \tag{22}$$

where $C(\mathbf{v})$ is the covariance of $\mathbb{X}$ and p is the coverage probability of $\mathbb{X}$.

This relation leads to improved estimators of GBL (Section 4) and shows that all the information summarised in the GBL of a stationary RACS $\mathbb{X}$ is contained in the covariance of $\mathbb{X}$. Furthermore, using (22), GBL can be easily calculated for intersections, unions and invertible linear transformations of independent stationary RACS with known covariance (Table 1 in supplementary material), and computed for a few parametric RACS models, such as Boolean models (Chiu et al., 2013, §3) (and the closely related random trema models (Mandelbrot, 1983, §33) with finite scale), impenetrable particles (Quintanilla, 1999), excursion sets of stationary Gaussian random and others (Torquato, 2002). The latter property potentially makes it possible to use GBL for model diagnostics, or for fitting models through minimum contrast (Chiu et al., 2013, §3.4.3), which is similar to the method of moments.

Proof of (22) We start with a relation for the first moment in (17). By Robbins' formula, an application of Fubini's Theorem (Robbins, 1944, 1947; Kolmogoroff and Leontowitsch, 1933; Kolmogorov and Leontovitch, 1992),

$$\begin{aligned}\mathbb{E}[|\mathbb{X} \cap B|] &= \mathbb{E}\left[\int_{\mathbb{R}^d} \mathbf{1}_{\mathbb{X}}(\mathbf{x})\mathbf{1}_B(\mathbf{x})\,\mathrm{d}\mathbf{x}\right] = \int_{\mathbb{R}^d} \mathbb{E}\left[\mathbf{1}_{\mathbb{X}}(\mathbf{x})\mathbf{1}_B(\mathbf{x})\right]\,\mathrm{d}\mathbf{x}\\ &= \int_{\mathbb{R}^d} P(\mathbf{x} \in \mathbb{X})\mathbf{1}_B(\mathbf{x})\,\mathrm{d}\mathbf{x} = \int_{\mathbb{R}^d} p\mathbf{1}_B(\mathbf{x})\,\mathrm{d}\mathbf{x} = p|B|, \end{aligned} \tag{23}$$

where p is the coverage probability of $\mathbb{X}$.

Using the second order Robbins' formula (Robbins, 1944) and similar arguments, the variance of $|\mathbb{X} \cap B|$ is (Molchanov, 1997, eq. 3.5),

$$\begin{aligned}\mathrm{Var}\left(|\mathbb{X} \cap B|\right) &= \int_{\mathbb{R}^d}\int_{\mathbb{R}^d} (C(\mathbf{x}-\mathbf{y}) - p^2)\mathbf{1}_B(\mathbf{x})\mathbf{1}_B(\mathbf{y})\,\mathrm{d}\mathbf{x}\,\mathrm{d}\mathbf{y}\\ &= \int_{\mathbb{R}^d} \gamma_B(\mathbf{v})C(\mathbf{v})\,\mathrm{d}\mathbf{v} - p^2|B|^2. \end{aligned} \tag{24}$$

Substituting (23) and (24) into the (random set) definition of GBL (17) gives (22) and completes the proof.

4 New Estimators of GBL

Here we use relation (22) to develop estimators of GBL that avoid the difficulties of the gliding box estimator with the observation window, mentioned in Section 2.2. Our estimators are also trivial to implement for non-rectangular 'boxes' B and can be computationally competitive with $\widehat{\mathrm{L}}_{\mathrm{GB}}$ (see Section G of the supplementary material).

Definition 3 *Suppose $\mathbb{X}$ is a stationary RACS with positive coverage probability and a realisation, X, of $\mathbb{X}$ is observed in a window W. We define the following GBL estimators by substituting estimators of coverage probability, covariance, centred covariance and pair* *correlation (Section 2.1.2) into* (22)*,*

$$\widehat{\mathrm{L}}_C(B) := \frac{1}{\hat{p}^2|B|^2}\int_{\mathbb{R}^d}\gamma_B(\mathbf{v})\hat{C}(\mathbf{v})\ \mathrm{d}\mathbf{v} = \frac{|W|^2}{|X\cap W|^2|B|^2}\int_{\mathbb{R}^d}\gamma_B(\mathbf{v})\frac{\gamma_{X\cap W}(\mathbf{v})}{\gamma_W(\mathbf{v})}\ \mathrm{d}\mathbf{v} \tag{25}$$

$$\widehat{\mathrm{L}}_{\kappa I}(B) = \frac{1}{\hat{p}^2|B|^2}\int_{\mathbb{R}^d}\gamma_B(\mathbf{v})\hat{\kappa}_I(\mathbf{v})\ \mathrm{d}\mathbf{v} + 1 \tag{26}$$

$$\widehat{\mathrm{L}}_{\kappa H}(B) = \frac{1}{\hat{p}^2|B|^2}\int_{\mathbb{R}^d}\gamma_B(\mathbf{v})\hat{\kappa}_H(\mathbf{v})\ \mathrm{d}\mathbf{v} + 1 = \frac{1}{|B|^2}\int_{\mathbb{R}^d}\gamma_B(\mathbf{v})\hat{g}_H(\mathbf{v})\ \mathrm{d}\mathbf{v} \tag{27}$$

$$\widehat{\mathrm{L}}_{\kappa M}(B) = \frac{1}{\hat{p}^2|B|^2}\int_{\mathbb{R}^d}\gamma_B(\mathbf{v})\hat{\kappa}_M(\mathbf{v})\ \mathrm{d}\mathbf{v} + 1 \tag{28}$$

$$\widehat{\mathrm{L}}_{gI}(B) = \frac{1}{|B|^2}\int_{\mathbb{R}^d}\gamma_B(\mathbf{v})\hat{g}_I(\mathbf{v})\ \mathrm{d}\mathbf{v} \tag{29}$$

$$\widehat{\mathrm{L}}_{gM}(B) = \frac{1}{|B|^2}\int_{\mathbb{R}^d}\gamma_B(\mathbf{v})\hat{g}_M(\mathbf{v})\ \mathrm{d}\mathbf{v}. \tag{30}$$

We call $\widehat{\mathrm{L}}_{\kappa H}$*,* $\widehat{\mathrm{L}}_{\kappa I}$*,* $\widehat{\mathrm{L}}_{\kappa M}$*,* $\widehat{\mathrm{L}}_{gI}$ *and* $\widehat{\mathrm{L}}_{gM}$*,* balanced covariance-based *estimators as each is based on Picka's balanced estimators.*

These estimators do not require the box B to be placed entirely within the observation window. Thus these estimators use data near the boundary of the observation window more efficiently than $\widehat{\mathrm{L}}_{\mathrm{GB}}$, and, for complicated observation windows, are able to produce GBL estimates for boxes much larger than $\widehat{\mathrm{L}}_{\mathrm{GB}}$.

In Section 5 we investigate the bias and variance of these estimators using simulations, because the variance, which is a fourth-order property of $\mathbb{X}$, is difficult to assess analytically. It is possible that our new estimators will give values less than 1 for large box sizes in some situations, although we have only observed this occurring significantly for $\widehat{\mathrm{L}}_C$, $\widehat{\mathrm{L}}_{gI}$ and $\widehat{\mathrm{L}}_{gM}$.

A counterpart to (22) for the fixed set scenario is the property that, in the absence of window edge effects, our new estimators give the same results to $\widehat{\mathrm{L}}_{\mathrm{GB}}$ as it then follows that $\widehat{\mathrm{L}}_{\mathrm{GB}}$ is approximately a function of $\hat{C}(\mathbf{v})$. We show this by defining the estimators,

$$\widehat{\mathrm{L}}^*_C(B, X) := \frac{1}{\hat{p}^2|B|^2}\int_{\mathbb{R}^d}\gamma_B(\mathbf{v})\frac{\gamma_{X\cap W}(\mathbf{v})}{|W|}\ \mathrm{d}\mathbf{v} \tag{31}$$

and

$$\widehat{\mathrm{L}}^*_{\mathrm{GB}}(\mathbf{B}, X) := \frac{\int_{\mathbb{R}^d} |X \cap (B \oplus \mathbf{y})|^2 \,\mathrm{d}\mathbf{y}/|W|}{\left(\int_{\mathbb{R}^d} |X \cap (B \oplus \mathbf{y})| \,\mathrm{d}\mathbf{y}/|W|\right)^2}, \tag{32}$$

which are equivalent to $\widehat{\mathrm{L}}_C$ and $\widehat{\mathrm{L}}_{\mathrm{GB}}$, respectively, in the absence of window edge effects. These estimators can be obtained from $\widehat{\mathrm{L}}_C$ and $\widehat{\mathrm{L}}_{\mathrm{GB}}$ by replacing $\gamma_W(\mathbf{v})$, and the first and second moment, (15) and (16), with $|W|$, $\int_{\mathbb{R}^d} |X \cap (B \oplus \mathbf{y})| \,\mathrm{d}\mathbf{y}/|W|$ and $\int_{\mathbb{R}^d} |X \cap (B \oplus \mathbf{y})|^2 \,\mathrm{d}\mathbf{y}/|W|$, respectively. It is then sufficient to show that $\widehat{\mathrm{L}}^*_C$ and $\widehat{\mathrm{L}}^*_{\mathrm{GB}}$ are mathematically equivalent for an arbitrary set X with positive finite volume. The relation extends to $\widehat{\mathrm{L}}_{\kappa H}$, $\widehat{\mathrm{L}}_{\kappa I}$, $\widehat{\mathrm{L}}_{\kappa M}$, $\widehat{\mathrm{L}}_{gI}$ and $\widehat{\mathrm{L}}_{gM}$ because $\hat{p}_R(\mathbf{v})$ is equivalent to $\hat{p}$ in the absence of window edge effects. In the supplementary material we provide an exact relation between $\widehat{\mathrm{L}}_{\mathrm{GB}}$ and the estimators (6) and (7).

Theorem 2 *Suppose that the set $X \subseteq \mathbb{R}^d$ has positive volume and that B is a bounded subset of $\mathbb{R}^d$, also with positive volume, then*

$$\widehat{\mathrm{L}}^*_{GB}(B) = \widehat{\mathrm{L}}^*_C(B) = \frac{1}{\hat{p}^2|B|^2} \int_{\mathbb{R}^d} \gamma_B(\mathbf{v}) \frac{\gamma_{X\cap W}(\mathbf{v})}{|W|} \,\mathrm{d}\mathbf{v}. \tag{33}$$

The proof of (33) proceeds similarly to the proof of (22). We include it in the appendix for completeness.

5 Simulation Study

The variance of a GBL estimator is a complicated fourth-order property that is difficult to compute analytically. Previous studies into the variance of GBL estimators (Feagin et al., 2007; Kirkpatrick and Weishampel, 2005), centred covariance estimators and pair correlation estimators (Picka, 1997, 2000; Mattfeldt and Stoyan, 2000) have used simulations, although some asymptotic results were achieved by Picka.

In this simulation study we consider three scenarios: in *Scenario 1* the observation window is fixed and the foreground is random; in *Scenario 2* the foreground is fixed and the observation window is random; and in *Scenario 3* both the foreground and observation window are random. Examples of these scenarios are, respectively, (Scenario 1) studies that have a predetermined observation window, like an urban area excluding water bodies (Sui and Wu, 2006), (Scenario 2) a time series of presence-absence maps with different patterns of occlusions affecting the observations, and (Scenario 3) a tissue sample that contains randomly located blood vessels and other items that are not of interest.

A brief description of the methods and a summary of the results are given below. Further details and analyses are available in Section D of the supplementary material. Results of the simulation study suggest that our balanced covariance-based estimators outperform $\widehat{\mathrm{L}}_{\mathrm{GB}}$ in all scenarios.

5.1 Methods and Selected Results

The foreground random set was taken to be a Boolean model of discs in $\mathbb{R}^2$, that is, the union of randomly-sized discs centred at the points of a homogeneous Poisson point process with an intensity of 0.05 points per unit area (Chiu et al., 2013, §2,§3), (Molchanov, 1997). The disc radii were independent and identically distributed with probability density $f(r) = k/r^3$ for $1 < r < 50$ and $f(r) = 0$ otherwise, where $k = 5000/2499$ is the normalising constant. This model, $\mathbb{X}$, was similar to the disc tremas of Mandelbrot (1983, §33) and thus exhibited some multiscale behaviour.

The simulations generated realisations of $\mathbb{X}$ inside a square study region Z of side length 200 units, with various levels of occlusions that prevented full observation of $\mathbb{X}$ in Z. For Scenario 1 we considered the case when Z was fully observed and multiple cases of Z partially occluded. For Scenario 2 we observed a single realisation, X, of $\mathbb{X}$ subject to random occlusions, $\mathbb{O}$, that covered on average 7.6% of Z. For Scenario 3 we simulated both $\mathbb{X}$ and $\mathbb{O}$. The study region Z with different patterns of occlusions is shown with example realisations of $\mathbb{X}$ in Figure 2.

Shown in Figure 3 is the pointwise mean and pointwise variance of $\widehat{\mathrm{L}}_{\mathrm{GB}}$, and each of our estimators given square boxes, B, for Scenario 3 and for selected fixed observation windows in Scenario 1. The pointwise mean and pointwise variance of the estimators for Scenario 2 (fixed foreground scenario) are shown in Figure 4. In Figure 3 and Figure 4 the

GBL of $\mathbb{X}$ was computed from model parameters using (22) and covariance formulae for Boolean models (Chiu et al., 2013, eq. 3.18). Note that, following conventional procedure, $\widehat{\mathrm{L}}_{\mathrm{GB}}$ was applied by replacing the region of interest in (15) and (16) with the observation window.

[Figure 2 about here.]

5.2 Summary of Results

The balanced covariance-based estimators, $\widehat{\mathrm{L}}_{\kappa H}$, $\widehat{\mathrm{L}}_{\kappa I}$, $\widehat{\mathrm{L}}_{\kappa M}$, $\widehat{\mathrm{L}}_{gI}$ and $\widehat{\mathrm{L}}_{gM}$, were indistinguishable in most cases. In every scenario that involved occlusions, these estimators were well-defined over a much larger range of box widths than $\widehat{\mathrm{L}}_{\mathrm{GB}}$, had the smallest bias, and, except for small intervals of box widths, the smallest variance. The variance of these estimators in fixed observation windows (Scenario 1) increased by at most a factor of 0.5 in the presence of occlusions that covered up to 50% of the study region; this variance was roughly 25 times the variance of the same estimators in Scenario 2 (fixed foreground and random occlusions), and did not substantially increase in Scenario 3 (random foreground and random occlusions). In comparison, for example, the occlusion pattern that covered 50% of the study region increased the variance of $\widehat{\mathrm{L}}_{\mathrm{GB}}$ for some boxes by a factor of 14. When Z was fully observed there were minimal differences between $\widehat{\mathrm{L}}_{\mathrm{GB}}$ and these balanced covariance-based estimators.

No estimators performed well when the study region was 90% covered by occlusions, nor on a square observation window with width substantially shorter than the maximum interaction distance of $\mathbb{X}$ (see Section D of the supplementary material).

[Figure 3 about here.]

[Figure 4 about here.]

6 Applications to Fragmented Forest Cover

According to Griffith (2004), summaries of changes in land-cover proportions (which are coverage probability estimates) do not adequately capture important changes in ecological functions such as forest connectivity and species movement, and landscape pattern change should be part of any land cover change monitoring program. Griffith further suggests that there is a practical need to focus on the dominant land cover type, for example forests, of any ecoregion. An example of such analysis was provided by Pintilii et al. (2017) who examined the fragmentation of forests as an indication of the extent of deforestation at a county level using multi-year global forest presence-absence classifications derived from Landsat satellite data. They found that applying a lacunarity index which was a summary of GBL[1], provided information for forest management strategies additional to the information provided by simply considering deforestation rates. Niemelä (1999) note that forest disturbances occur at different scales and can differ substantially in ecological effect.

Here we present examples of the use of our GBL estimators at two different scales. In the first example we examine the stability of GBL estimators as they would be applied in meso-scale forest fragmentation studies that use time-series data obtained from optical spaceborne sensors, such as the Landsat satellites. Patterns of missing ground observations due to occlusions by clouds are normal for these sensors, with further omissions created by some sensors with documented hardware problems, such as Landsat 7 (U. S. Geological Survey, 2016). Robustness or resistance to these effects is crucial to applications.

In the second example, we consider localised forest degradation by examining the GBL of tree canopies at the interface of natural forest systems and urban development. Here the forests are subject to disturbance through removal for urban development, natural fires, planned burns to reduce fuel loads, and disease (Shearer et al., 2007).

6.1 Stability of estimators applied at meso-scale in the presence of missing data

We applied $\widehat{\mathrm{L}}_{\mathrm{GB}}$, defined in (14), and our new GBL estimators (25)–(30) to presence-absence maps of forest (Figure 5 bottom) extracted from seven satellite photographs (Figure 5 top) captured by Landsat 7 and Landsat 8 of the same $18.8km \times 18.8km$ study

[1]Ion Andronache, Personal communication, August 3 2018

region in South-West Australia. The photographs were captured from December 2015 to March 2016 within the same hot dry summer so that the forest cover pattern of the region was close to identical at each date of capture. Differences in the GBL estimates between the forest maps can thus be attributed to differences in the observation windows caused by clouds and a sensor malfunction.

The study region was only fully observed in the photograph captured on February 26th; all other photographs contained cloud or suffered periodic missing data due to Landsat 7's SLC-off hardware issue (U. S. Geological Survey, 2016). The same procedure, which used spectral values, was used to convert all photographs except December 16th's into forest maps. The December 16th photograph was the only photograph captured by Landsat 7 and received a comparable procedure designed to minimise the differences between the forest maps.

The balanced covariance-based estimates from the different maps were substantially more alike than estimates using either $\widehat{\mathrm{L}}_C$ or $\widehat{\mathrm{L}}_{\mathrm{GB}}$, and produced estimates for much larger box widths than $\widehat{\mathrm{L}}_{\mathrm{GB}}$ for all partial observations of the study region (Figure 6). Excluding estimates from the December 8th and December 16th maps, the average integrated squared discrepancy (ISD) of $\widehat{\mathrm{L}}_{\mathrm{GB}}$ for boxes from $25m$ (1 pixel) to 1.8km (1/10th of the width of the study region) was more than four times the average ISD of each balanced covariance-based estimator, and three times the average ISD of $\widehat{\mathrm{L}}_C$ (Table 1). The average ISD was computed relative to the GBL estimates from the fully observed study region (February 26th map), and estimates from the December 8th and December 16th maps were excluded as $\widehat{\mathrm{L}}_{\mathrm{GB}}$ did not produce estimates for all boxes up to 1.8km wide for these maps.

For each map the GBL estimates given square boxes with widths from 1 pixel (25m) to just over a quarter of the region's width (5km) are shown in Figure 7. Log-log plots of estimated $\mathrm{L}(B)$, favoured by Plotnick et al. (1996), are included. Slight differences between the centred covariance-based estimates, from $\widehat{\mathrm{L}}_{\kappa H}$, $\widehat{\mathrm{L}}_{\kappa I}$ and $\widehat{\mathrm{L}}_{\kappa M}$, and the pair correlation based estimates, from $\widehat{\mathrm{L}}_{gI}$ and $\widehat{\mathrm{L}}_{gM}$, can be seen for most maps. The estimators produced results most similar to each other for the fully observed study region (February 26th map), which had the largest, simplest observation window and thus the smallest observation window edge effects.

The data and R code used for this example are included in the supplementary material.

[Figure 5 about here.]

[Figure 6 about here.]

[Table 1 about here.]

[Figure 7 about here.]

6.2 Estimators applied to forest disturbance at local scale

We estimated the GBL of tree canopy cover for 33 forested land parcels subject to disturbance through fire and development. Of the 33 parcels, 27 were selected from native forest, and 6 'settlement' parcels were selected from the boundary of native forest and human development. These 'settlement' parcels were subject to partial removal of forest for dwellings and grassed areas. The native forest cover is dynamic, in large part because it is subject to prescribed burning for management of fuel load (Boer et al., 2009), and the 27 native forest parcels were labelled according to whether they were decreasing, recovering or increasing in cover for the period 1990-2016. The labels were made possible through cover trend information derived from the Landsat sensor (Wallace et al., 2006). Tree canopy presence-absence maps with 20cm spatial resolution were generated for each parcel from aerial photography captured in February 2016 following the methods described by Caccetta et al. (2015).

The densities in the native forest parcels overlap with those of the 'settlement' parcels, providing an opportunity to compare the metrics for sites undergoing different disturbances but having similar densities. Illustrating this the $\widehat{\mathrm{L}}_{\kappa H}$ estimates of GBL from the tree canopy presence absence maps of the 33 parcels are provided in Figure 8 and selected parcels of comparable density are depicted in Figure 9. The estimates are presented in Figure 8 transformed to $\big(\widehat{\mathrm{L}}_{\kappa H}(B)-1\big)\hat{p}/(1-\hat{p})$, which standardised the estimates to 1 for arbitrarily small boxes and 0 when the box equals the observation window. From Figure 8 (right), we observe much overlap in the range of curves for parcels labelled as decreasing, recovering and increasing (in cover), which is not so surprising given that these labels are based on all cover (including non-tree ground covers) as opposed to tree cover, which we are examining. We further observe some separation of curves for the native forests with various levels of disturbance from the curves for the settlements parcels. From Figure 8, left and centre, we observe a similar separation of the settlement parcels from native forest parcels having comparable tree canopy densities, reflecting the change in spatial tree arrangement in settlement versus native forested regions and a possible metric for assessing or detecting settlements and their level of impact.

Estimates using the other GBL estimators are in Section F of the supplementary material. For these parcels, and the given box widths, we found that our new estimators were computationally competitive with the gliding box estimator. The centred covariance-based estimates, from $\widehat{\mathrm{L}}_{\kappa H}$, $\widehat{\mathrm{L}}_{\kappa I}$ and $\widehat{\mathrm{L}}_{\kappa M}$, were nearly identical to each other, and the differences to the $\widehat{\mathrm{L}}_{\mathrm{GB}}$ estimates did not affect interpretation. For some parcels the estimates from $\widehat{\mathrm{L}}_{C}$, $\widehat{\mathrm{L}}_{gI}$ and $\widehat{\mathrm{L}}_{gM}$ were poorly behaved. This seemed related to an incompatibility, unique to $\widehat{\mathrm{L}}_{C}$, $\widehat{\mathrm{L}}_{gI}$ and $\widehat{\mathrm{L}}_{gM}$, of GBL estimates from the presence-absence maps where the foreground is swapped with the background and may warrant further investigation.

[Figure 8 about here.]

[Figure 9 about here.]

7 Conclusion

In this paper we showed that the GBL of a stationary random closed set (RACS) with positive coverage probability is related to its covariance. We used this relation to propose new estimators of GBL that operate seamlessly in complicated observation windows. These estimators remove the obligation of the scientist to reconstruct occluded sections of patterns and, for example, enable estimates of GBL from Earth observation data that contains many clouds. We tested and demonstrated our new GBL estimators on simulated binary maps, forest maps derived from satellite photography, and decimetre resolution tree canopy maps.

The best-performing GBL estimators were our new balanced, centred covariance-based estimators, $\widehat{\mathrm{L}}_{\kappa H}$, $\widehat{\mathrm{L}}_{\kappa I}$ and $\widehat{\mathrm{L}}_{\kappa M}$. These estimators operated on binary maps with irregular observation windows for much larger boxes than the traditional gliding box estimator $\widehat{\mathrm{L}}_{\mathrm{GB}}$, produced estimates with average integrated squared discrepancies less than a quarter that of the $\widehat{\mathrm{L}}_{\mathrm{GB}}$ estimates for our satellite photography example, increased variance by at most a factor of 0.5 for simulated observations with 50% occlusions, where as in the same situation the variance of the $\widehat{\mathrm{L}}_{\mathrm{GB}}$ increased by a factor of 14 for some box sizes, had smaller variance than $\widehat{\mathrm{L}}_{C}$ in nearly all situations, and produced estimates with better behaviour than our balanced pair correlation based estimators, $\widehat{\mathrm{L}}_{C}$, $\widehat{\mathrm{L}}_{gI}$ and $\widehat{\mathrm{L}}_{gM}$, in the decimetre resolution tree canopy example. Estimators with further reductions in variance might be obtained for stationary RACS with rotation invariant distributions using isotropic centred covariance and pair correlation estimators (Picka, 2000; Mattfeldt and Stoyan, 2000).

Our relationship between GBL and covariance enables the GBL of intersections and unions of stationary RACS to be calculated from the covariance of the original sets, and allows the GBL of some RACS models to be calculated directly from parameters without simulation, which, for example, allowed us to easily assess the bias of GBL estimators in our simulation study.

The relation between GBL and covariance, and the analogous relation between $\widehat{\mathrm{L}}_{\mathrm{GB}}$ and $\widehat{\mathrm{L}}_{C}$ in the absence of window edge effects, show that GBL and covariance are closely related in theory and in applications. Covariance may be a good alternative to GBL as covariance (or estimated covariance) contains all the information about a process (or pattern) that GBL contains, covariance is easily interpretable as the probability of a pair of points being in the set, and the covariance of sets created by intersections, unions and invertible linear transformations may be calculated from the covariance of the original sets. However GBL has wide existing applications, and our high resolution tree canopy example suggested that GBL estimates could be useful for investigating local scale forest disturbance. Further research is needed to determine whether covariance could equal the performance of GBL in these applications.

Relations between fractal analysis tools and non-fractal analysis tools, such as the relation between GBL and covariance that this paper contributes, are valuable for applying spatial pattern analysis tools (Sun et al., 2006). There are other relations between popular fractal tools and spatial statistics that do not appear to be widely used, such as a characterisation of common Rényi dimension estimators as using power-law approximations to the results of reduced moment measure estimators of spatial point processes (Vere-Jones, 1999) and common box-counting dimension estimators using power-law approximations to the results of contact distribution estimators.[2]

An R package for computing our new estimators and the gliding box estimator is included in the supplementary material.

Appendix

Proof of (33) The volume $|X \cap (B \oplus \mathbf{y})|$ can be written as an integral of indicator functions

$$|X \cap (B \oplus \mathbf{y})| = \int_{\mathbb{R}^d} \mathbf{1}_{X\cap W}(\mathbf{x}) \mathbf{1}_{B\oplus\mathbf{y}}(\mathbf{x}) \,\mathrm{d}\mathbf{x} = \int_{\mathbb{R}^d} \mathbf{1}_W(\mathbf{x}) \mathbf{1}_X(\mathbf{x}) \mathbf{1}_B(\mathbf{x}-\mathbf{y}) \,\mathrm{d}\mathbf{x}.$$

so the first moment is (using the Fubini-Tonelli theorem)

$$\begin{aligned}\frac{1}{|W|}\int_{\mathbb{R}^d} |X \cap (B \oplus \mathbf{y})| \,\mathrm{d}\mathbf{y} &= \frac{1}{|W|}\int_{\mathbb{R}^d}\int_{\mathbb{R}^d} \mathbf{1}_W(\mathbf{x}) \mathbf{1}_X(\mathbf{x}) \mathbf{1}_B(\mathbf{x}-\mathbf{y}) \,\mathrm{d}\mathbf{x}\,\mathrm{d}\mathbf{y} \\ &= \frac{1}{|W|}\int_{\mathbb{R}^d} \mathbf{1}_W(\mathbf{x}) \mathbf{1}_X(\mathbf{x}) \int_{\mathbb{R}^d} \mathbf{1}_B(\mathbf{x}-\mathbf{y}) \,\mathrm{d}\mathbf{y}\,\mathrm{d}\mathbf{x} \\ &= \frac{|X\cap W|}{|W|}|B| = \hat{p}|B|. \end{aligned} \tag{34}$$

[2]The latter does not appear to be explicitly noted in the literature and will be discussed fully elsewhere - it seems likely that authors such as Serra (1982, p151) and Vere-Jones (1999) were aware of the connection

With similar arguments the second moment is

$$\begin{aligned}
&\frac{1}{|W|}\int_{\mathbb{R}^d}|X\cap(B\oplus\mathbf{y})|^2\,\mathrm{d}\mathbf{y}\\
&\qquad=\frac{1}{|W|}\int_{\mathbb{R}^d}\int_{\mathbb{R}^d}\mathbf{1}_W(\mathbf{x})\mathbf{1}_X(\mathbf{x})\mathbf{1}_B(\mathbf{x}-\mathbf{y})\,\mathrm{d}\mathbf{x}\int_{\mathbb{R}^d}\mathbf{1}_W(\mathbf{z})\mathbf{1}_X(\mathbf{z})\mathbf{1}_B(\mathbf{z}-\mathbf{y})\,\mathrm{d}\mathbf{z}\;\mathrm{d}\mathbf{y}\\
&\qquad=\frac{1}{|W|}\int_{\mathbb{R}^d}\int_{\mathbb{R}^d}\mathbf{1}_W(\mathbf{x})\mathbf{1}_X(\mathbf{x})\mathbf{1}_W(\mathbf{z})\mathbf{1}_X(\mathbf{z})\int_{\mathbb{R}^d}\mathbf{1}_B(\mathbf{x}-\mathbf{y})\mathbf{1}_B(\mathbf{z}-\mathbf{y})\,\mathrm{d}\mathbf{y}\;\mathrm{d}\mathbf{x}\;\mathrm{d}\mathbf{z}\\
&\qquad=\frac{1}{|W|}\int_{\mathbb{R}^d}\int_{\mathbb{R}^d}\mathbf{1}_W(\mathbf{x})\mathbf{1}_X(\mathbf{x})\mathbf{1}_W(\mathbf{z})\mathbf{1}_X(\mathbf{z})\gamma_B(\mathbf{z}-\mathbf{x})\,\mathrm{d}\mathbf{x}\;\mathrm{d}\mathbf{z}\\
&\qquad=\frac{1}{|W|}\int_{\mathbb{R}^d}|((X\cap W)\oplus\mathbf{v})\cap(X\cap W)|\gamma_B(\mathbf{v})\,\mathrm{d}\mathbf{v}\\
&\qquad=\frac{1}{|W|}\int_{\mathbb{R}^d}\gamma_{X\cap W}(\mathbf{v})\gamma_B(\mathbf{v})\,\mathrm{d}\mathbf{v}=\int_{\mathbb{R}^d}\frac{\gamma_{X\cap W}(\mathbf{v})}{|W|}\gamma_B(\mathbf{v})\,\mathrm{d}\mathbf{v}.
\end{aligned}\tag{35}$$

Substitution of (34) and (35) into (32) proves statement (33).

References

Aghajanzadeh, S., Kashaninejad, M., and Ziaiifar, A. M. (2017), "Cloud stability of sour orange juice as affected by pectin methylesterase during come up time: Approached through fractal dimension," *International Journal of Food Properties*, 20(S3), S2508–S2519.

Allain, C., and Cloitre, M. (1991), "Characterizing the lacunarity of random and deterministic fractal sets," *Physical Review A*, 44(6), 3552–3558.

Anderson, J. K., Huang, J. Y., Wreden, C., Sweeney, E. G., Goers, J., Remington, S. J., and Guillemin, K. (2015), "Chemorepulsion from the Quorum Signal Autoinducer-2 Promotes Helicobacter pylori Biofilm Dispersal," *mBio*, 6(4). PMID: 26152582.

Anovitz, L. M., and Cole, D. R. (2015), "Characterization and Analysis of Porosity and Pore Structures," *Reviews in Mineralogy and Geochemistry*, 80(1), 61–164.

Aznarte, J. I., Iglesias-Parro, S., Ibáñez-Molina, A., and Soriano, M. F. (2014), A New Computational Measure for Detection of Extrapyramidal Symptoms,, in *Proceedings IWBBIO*, University of Grenada, Grenada, pp. 13–22.

Azzaz, N., and Haddad, B. (2017), "Classification of radar echoes using fractal geometry," *Chaos, Solitons & Fractals*, 98, 130–144.

Baddeley, A., and Jensen, E. B. V. (2005), *Stereology for Statisticians*, Vol. 103 of *Monographs on Statistics & Applied Probability*, Boca Raton, Florida: Chapman and Hall/CRC.

Baveye, P., Boast, C. W., Gaspard, S., Tarquis, A. M., and Millan, H. (2008), "Introduction to Fractal Geometry, Fragmentation Processes and Multifractal Measures: Theory and Operational Aspects of their Application to Natural Systems," in *Biophysical Chemistry of Fractal Structures and Processes in Environmental Systems*, England: Wiley-Blackwell, pp. 11–67. DOI: 10.1002/9780470511206.ch2.

Boer, M. M., Sadler, R. J., Wittkuhn, R. S., McCaw, L., and Grierson, P. F. (2009), "Long-term impacts of prescribed burning on regional extent and incidence of wildfires—Evidence from 50 years of active fire management in SW Australian forests," *Forest Ecology and Management*, 259(1), 132–142.

Borys, P., Krasowska, M., Grzywna, Z. J., Djamgoz, M. B. A., and Mycielska, M. E. (2008), "Lacunarity as a novel measure of cancer cells behavior," *Biosystems*, 94(3), 276–281.

Caccetta, P., Collings, S., Devereux, A., Hingee, K. L., McFarlane, D., Traylen, A., Wu, X., and Zhou, Z. (2015), "Monitoring land surface and cover in urban and peri-urban environments using digital aerial photography," *International Journal of Digital Earth*, pp. 1–19.

Chappard, D., Legrand, E., Haettich, B., Chalès, G., Auvinet, B., Eschard, J., Hamelin, J., Baslé, M., and Audran, M. (2001), "Fractal dimension of trabecular bone: comparison of three histomorphometric computed techniques for measuring the architectural two-dimensional complexity," *The Journal of Pathology*, 195(4), 515–521.

Cheng, Q. (1997), "Multifractal Modeling and Lacunarity Analysis," *Mathematical Geology*, 29(7), 919–932.

Chiu, S. N., Stoyan, D., Kendall, W. S., and Mecke, J. (2013), *Stochastic Geometry and Its Applications*, 3 edn, Chichester, United Kingdom: John Wiley & Sons.

Cumbrera, R., Tarquis, A. M., Gascó, G., and Millán, H. (2012), "Fractal scaling of apparent soil moisture estimated from vertical planes of Vertisol pit images," *Journal of Hydrology*, 452-453, 205–212.

Diaz, S., Casselbrant, I., Piitulainen, E., Magnusson, P., Peterson, B., Pickering, E., Tuthill, T., Ekberg, O., and Akeson, P. (2009), "Progression of Emphysema in a 12-month Hyperpolarized 3He-MRI Study: Lacunarity Analysis Provided a More Sensitive Measure than Standard ADC Analysis1," *Academic Radiology*, 16(6), 700–707.

Diggle, P. J. (1981), "Binary Mosaics and the Spatial Pattern of Heather," *Biometrics*, 37(3), 531–539.

Dong, P. (2000), "Test of a new lacunarity estimation method for image texture analysis," *International Journal of Remote Sensing*, 21(17), 3369–3373.

Dàvila, E., and Parés, D. (2007), "Structure of heat-induced plasma protein gels studied by fractal and lacunarity analysis," *Food Hydrocolloids*, 21(2), 147–153.

Feagin, R. A., Wu, X. B., and Feagin, T. (2007), "Edge effects in lacunarity analysis," *Ecological Modelling*, 201(3–4), 262–268.

Gould, D. J., Vadakkan, T. J., Poché, R. A., and Dickinson, M. E. (2011), "Multifractal and Lacunarity Analysis of Microvascular Morphology and Remodeling," *Microcirculation*, 18(2), 136–151.

Griffith, J. A. (2004), "The role of landscape pattern analysis in understanding concepts of land cover change," *Journal of Geographical Sciences*, 14(1), 3.

Karperien, A., Ahammer, H., and Jelinek, H. F. (2013), "Quantitating the subtleties of microglial morphology with fractal analysis," *Frontiers in Cellular Neuroscience*, 7.

Karperien, A. L. (2005), FracLac's Advanced User Manual,, Technical report, Charles Sturt University. Version 2.0f.

Kautz, M., Düll, J., and Ohser, J. (2011), "Spatial dependence of random sets and its application to disperion of bark beetle infestation in a natural forest.," *Image Analysis & Stereology*, 30(3), 123–131.

Kirkpatrick, L. A., and Weishampel, J. F. (2005), "Quantifying spatial structure of volumetric neutral models," *Ecological Modelling*, 186(3), 312–325.

Koch, K., Ohser, J., and Schladitz, K. (2003), "Spectral Theory for Random Closed Sets and Estimating the Covariance via Frequency Space," *Advances in Applied Probability*, 35(3), 603–613.

Kolmogoroff, A., and Leontowitsch, M. (1933), "Zur Berechnung der mittleren Brownschen Fläche," *Physikalische Zeitschrift der Sowjetunion*, 4, 1–13.

Kolmogorov, A., and Leontovitch, M. (1992), "On computing the mean Brownian area," in *Selected works of A.N. Kolmogorov, Volume II: Probability and mathematical statistics*, ed. A. Shiryaev, Vol. 26 of *Mathematics and its applications (Soviet series)*, Dordrecht–Boston–London: Kluwer, pp. 128–138.

Lin, B., and Yang, Z. R. (1986), "A suggested lacunarity expression for Sierpinski carpets," *Journal of Physics A: Mathematical and General*, 19(2), L49.

Liu, C., and Zhang, W. (2010), Multiscale study on the spatial heterogeneity of remotely-sensed evapotranspiration in the typical Oasis of Tarim Basin,, in *Proceedings of the Sixth International Symposium on Digital Earth: Data Processing and Applications*, Vol. 7841, International Society for Optics and Photonics, Beijing, p. 78411A.

Mandelbrot, B. B. (1983), *Fractals and the Geometry of Nature*, New York: W. H. Freeman and Company.

Mandelbrot, B. B., and Stauffer, D. (1994), "Antipodal correlations and the texture (fractal lacunarity) in critical percolation clusters," *Journal of Physics A: Mathematical and General*, 27(9), L237.

Matheron, G. (1975), *Random sets and integral geometry*, USA: John Wiley & Sons.

Mattfeldt, T., and Stoyan, D. (2000), "Improved estimation of the pair correlation function of random sets," *Journal of Microscopy*, 200(2), 158–173.

McIntyre, N. E., and Wiens, J. A. (2000), "A novel use of the lacunarity index to discern landscape function," *Landscape Ecology*, 15(4), 313–321.

Molchanov, I. (1997), *Statistics of the Boolean Model for Practitioners and Mathematicians*, Chichester, United Kingdom: John Wiley & Sons.

Molchanov, I. S. (2005), *Theory of random sets*, Probability and its applications, London: Springer.

Myint, S. W., and Lam, N. (2005), "A study of lacunarity-based texture analysis approaches to improve urban image classification," *Computers, Environment and Urban Systems*, 29(5), 501–523.

Niemelä, J. (1999), "Management in relation to disturbance in the boreal forest," *Forest Ecology and Management*, 115(2), 127–134.

Nott, D. J., and Wilson, R. J. (2000), "Multi-phase image modelling with excursion sets," *Signal Processing*, 80(1), 125–139.

Owen, K. K. (2012), Geospatial and Remote Sensing-based Indicators of Settlement Type – Differentiating Informal and Formal Settlements in Guatemala City, PhD thesis, George Mason University.

Owen, K., and University, G. M. (2011), Settlement Indicators of Wellbeing and Economic Status - Lacunarity and Vegetation,, in *Proceedings of the Pecora 18 Symposium*, American Society for Photogrammetry and Remote Sensing, Virginia, USA.

Pendleton, D. E., Dathe, A., and Baveye, P. (2005), "Influence of image resolution and evaluation algorithm on estimates of the lacunarity of porous media," *Physical Review E*, 72(4), 041306.

Picka, J. D. (1997), Variance-reducing modifications for estimators of dependence in random sets, Ph.D., The University of Chicago, United States – Illinois.

Picka, J. D. (2000), "Variance Reducing Modifications for Estimators of Standardized Moments of Random Sets," *Advances in Applied Probability*, 32(3), 682–700.

Pintilii, R., Andronache, I., Diaconu, D. C., Dobrea, R. C., Zeleňáková, M., Fensholt, R., Peptenatu, D., Drăghici, C., and Ciobotaru, A. (2017), "Using Fractal Analysis in Modeling the Dynamics of Forest Areas and Economic Impact Assessment: Maramureș County, Romania, as a Case Study," *Forests*, 8(1), 25.

Plotnick, R. E., Gardner, R. H., Hargrove, W. W., Prestegaard, K., and Perlmutter, M. (1996), "Lacunarity analysis: A general technique for the analysis of spatial patterns," *Physical Review E*, 53(5), 5461–5468.

Plotnick, R. E., Gardner, R. H., and O'Neill, R. V. (1993), "Lacunarity indices as measures of landscape texture," *Landscape Ecology*, 8(3), 201–211.

Quintanilla, J. (1999), "Microstructure functions for random media with impenetrable particles," *Physical Review E*, 60(5), 5788–5794.

Quintanilla, J. A. (2008), "Necessary and sufficient conditions for the two-point phase probability function of two-phase random media," *Proceedings of the Royal Society of London A: Mathematical, Physical and Engineering Sciences*, 464(2095), 1761–1779.

Quintanilla, J. A., Chen, J. T., Reidy, R. F., and Allen, A. J. (2007), "Versatility and robustness of Gaussian random fields for modelling random media," *Modelling and Simulation in Materials Science and Engineering*, 15(4), S337.

Rankey, E. C. (2016), "On facies belts and facies mosaics: Holocene isolated platforms, South China Sea," *Sedimentology*, 63(7), 2190–2216.

Reiss, M. (2016), "frac2D: Fractal and Lacunarity methods for 2D digital images,".
URL: *https://sourceforge.net/projects/iqm-plugin-frac2d/*

Reiss, M. A., Lemmerer, B., Hanslmeier, A., and Ahammer, H. (2016), "Tug-of-war lacunarity—A novel approach for estimating lacunarity," *Chaos: An Interdisciplinary Journal of Nonlinear Science*, 26(11), 113102.

Robbins, H. (1947), "Acknowledgement of priority," *Annals of Mathematical Statistics*, 18, 297.

Robbins, H. E. (1944), "On the Measure of a Random Set," *The Annals of Mathematical Statistics*, 15(1), 70–74.

Roces-Díaz, J. V., Díaz-Varela, E. R., and Álvarez Álvarez, P. (2014), "Analysis of spatial scales for ecosystem services: Application of the lacunarity concept at landscape level in Galicia (NW Spain)," *Ecological Indicators*, 36, 495–507.

Schneider, R., and Weil, W. (2008), *Stochastic and Integral Geometry*, Probability and Its Applications, Germany: Springer-Verlag.

Serra, J. P. (1982), *Image analysis and mathematical morphology*, London ; New York: Academic Press.

Shah, R. G., Salafia, C. M., Girardi, T., and Merz, G. S. (2016), "Villus packing density and lacunarity: Markers of placental efficiency?," *Placenta*, 48, 68–71.

Shearer, B. L., Crane, C. E., Barrett, S., and Cochrane, A. (2007), "Phytophthora cinnamomi invasion, a major threatening process to conservation of flora diversity in the South-west Botanical Province of Western Australia," *Australian Journal of Botany*, 55(3), 225–238.

Stoyan, D., and Stoyan, H. (1994), *Fractals, Random Shapes and Point Fields: Methods of Geometrical Statistics*, Chichester, United Kingdom: John Wiley & Sons.

Sui, D. Z., and Wu, X. B. (2006), "Changing Patterns of Residential Segregation in a Prismatic Metropolis: A Lacunarity-Based Study in Houston, 1980–2000," *Environment and Planning B: Planning and Design*, 33(4), 559–579.

Sun, W., Xu, G., Gong, P., and Liang, S. (2006), "Fractal analysis of remotely sensed images: A review of methods and applications," *International Journal of Remote Sensing*, 27(22), 4963–4990.

Sung, C. Y., Yi, Y.-j., and Li, M. (2013), “Impervious surface regulation and urban sprawl as its unintended consequence,” *Land Use Policy*, 32(Supplement C), 317–323.

Torquato, S. (2002), *Random Heterogeneous Materials: Microstructure and Macroscopic Properties*, New York, USA: Springer. DOI: 10.1007/978-1-4757-6355-3.

U. S. Geological Survey (2016), “*SLC-off Products: Background*”. **URL:** *https://landsat.usgs.gov/slc-products-background* Accessed: 18th of April 2017.

Valous, N. A., Mendoza, F., Sun, D., and Allen, P. (2009), “Texture appearance characterization of pre-sliced pork ham images using fractal metrics: Fourier analysis dimension and lacunarity,” *Food Research International*, 42(3), 353–362.

Velazquez-Camilo, O., Bolaños-Reynoso, E., Rodriguez, E., and Alvarez-Ramirez, J. (2010), “Characterization of cane sugar crystallization using image fractal analysis,” *Journal of Food Engineering*, 100(1), 77–84.

Vere-Jones, D. (1999), “On the fractal dimensions of point patterns,” *Advances in Applied Probability*, 31(3), 643–663.

Voss, R. F. (1986), “Characterization and Measurement of Random Fractals,” *Physica Scripta*, 1986(T13), 27.

Wallace, J., Behn, G., and Furby, S. (2006), “Vegetation condition assessment and monitoring from sequences of satellite imagery,” *Ecological Management & Restoration*, 7(s1), S31–S36.

Xue, S., Wang, H., Yang, H., Yu, X., Bai, Y., Tendu, A. A., Xu, X., Ma, H., and Zhou, G. (2017), “Effects of high-pressure treatments on water characteristics and juiciness of rabbit meat sausages: Role of microstructure and chemical interactions,” *Innovative Food Science & Emerging Technologies*, 41, 150–159.

List of Figures

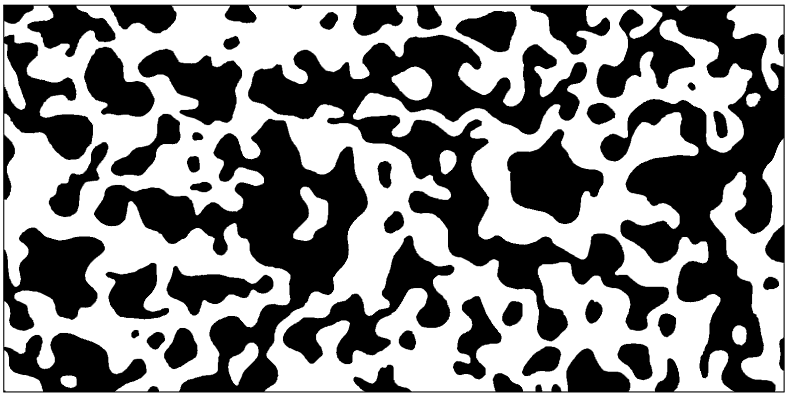

Figure 1: Presence (black) and absence (white) of the heather plant *Calluna vulgaris* in a 20 × 10 metre study region in Jädraås, Sweden (Diggle, 1981). The binary image, 1570 × 778 pixels, was scanned and cleaned by Chris Jonker, Henk Heijmans and Adrian Baddeley from the original hand-drawn map. Data available in the `spatstat` package.

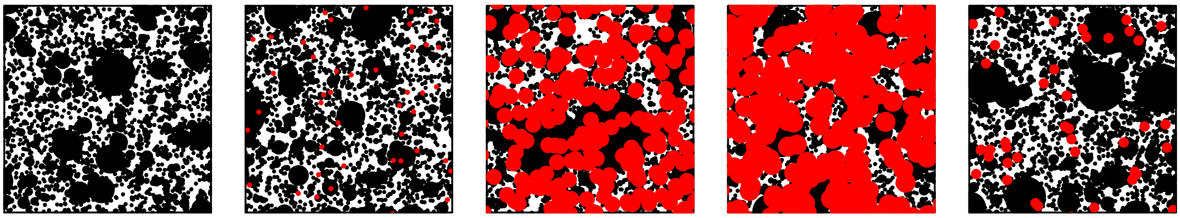

Figure 2: Example realisations of $\mathbb{X}$ in different observation windows. *From left:* The full study region Z; the study region Z with the fixed occlusion patterns that covered 2%, 50% and 70% of the study region; and Z with an example of the random occlusion process, $\mathbb{O}$, used in Scenario 2 and 3. Black: Foreground. White: Background. Red: Occlusions.

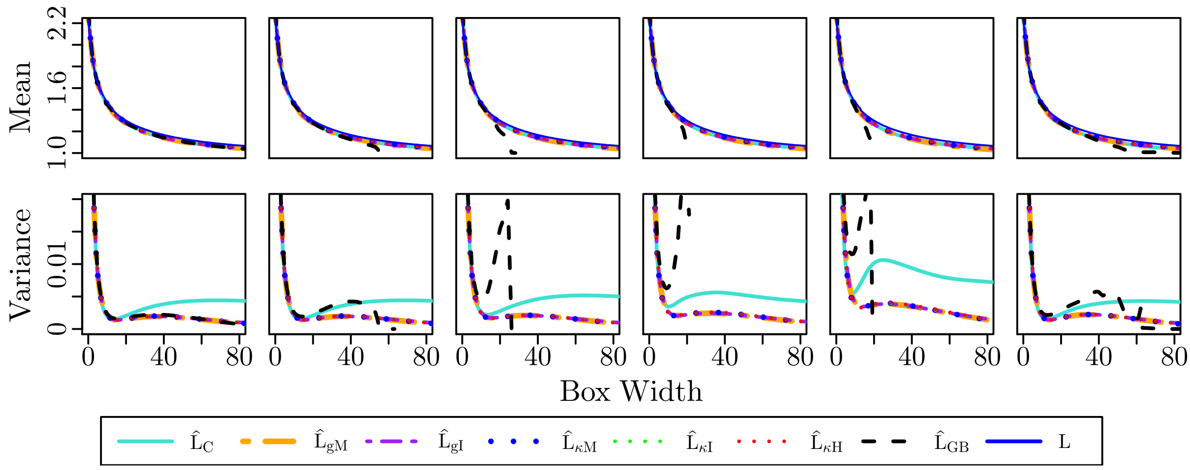

Figure 3: Pointwise mean (top) and pointwise variance (bottom) of GBL estimators. *From left:* The RACS $\mathbb{X}$ observed in the full study region Z; $\mathbb{X}$ observed in Z given the fixed occlusion patterns that covered 2%, 31%, 50% and 70% of the study region; and $\mathbb{X}$ observed in a random observation window (Scenario 3).

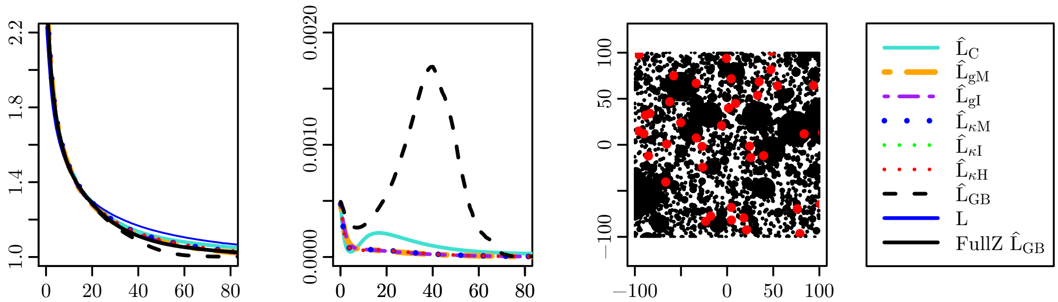

Figure 4: Pointwise mean (left) and pointwise variance (centre) of GBL estimators for Scenario 2 with the fixed realisation X of $\mathbb{X}$ (right). *In left - solid black line:* The $\widehat{L}_{GB}$ estimate from X fully observed in Z is shown as a solid black line. *In right - red:* An example occlusion pattern.

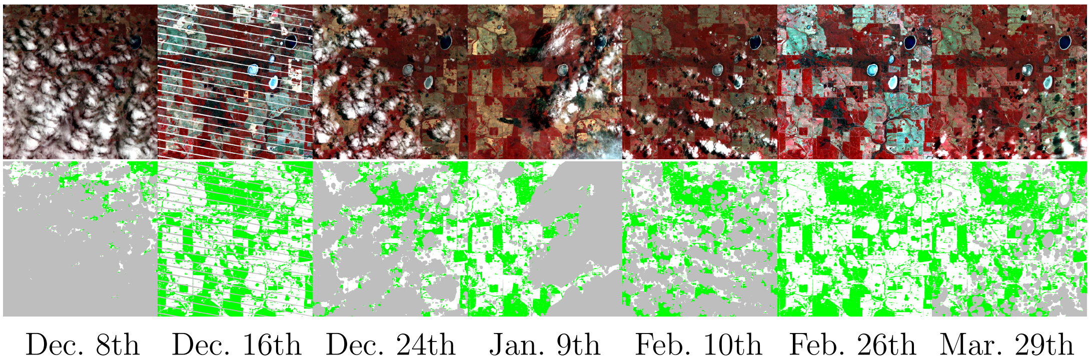

Figure 5: *Top:* The satellite photographs in false colour (specifically the displayed red, green and blue intensity corresponds to near-infrared, red and green light, respectively). *Bottom:* Forest masks derived from the photographs. Green: Forest. White: Not-forest. Grey: Missing data (due to cloud, cloud shadow or SLC-off).

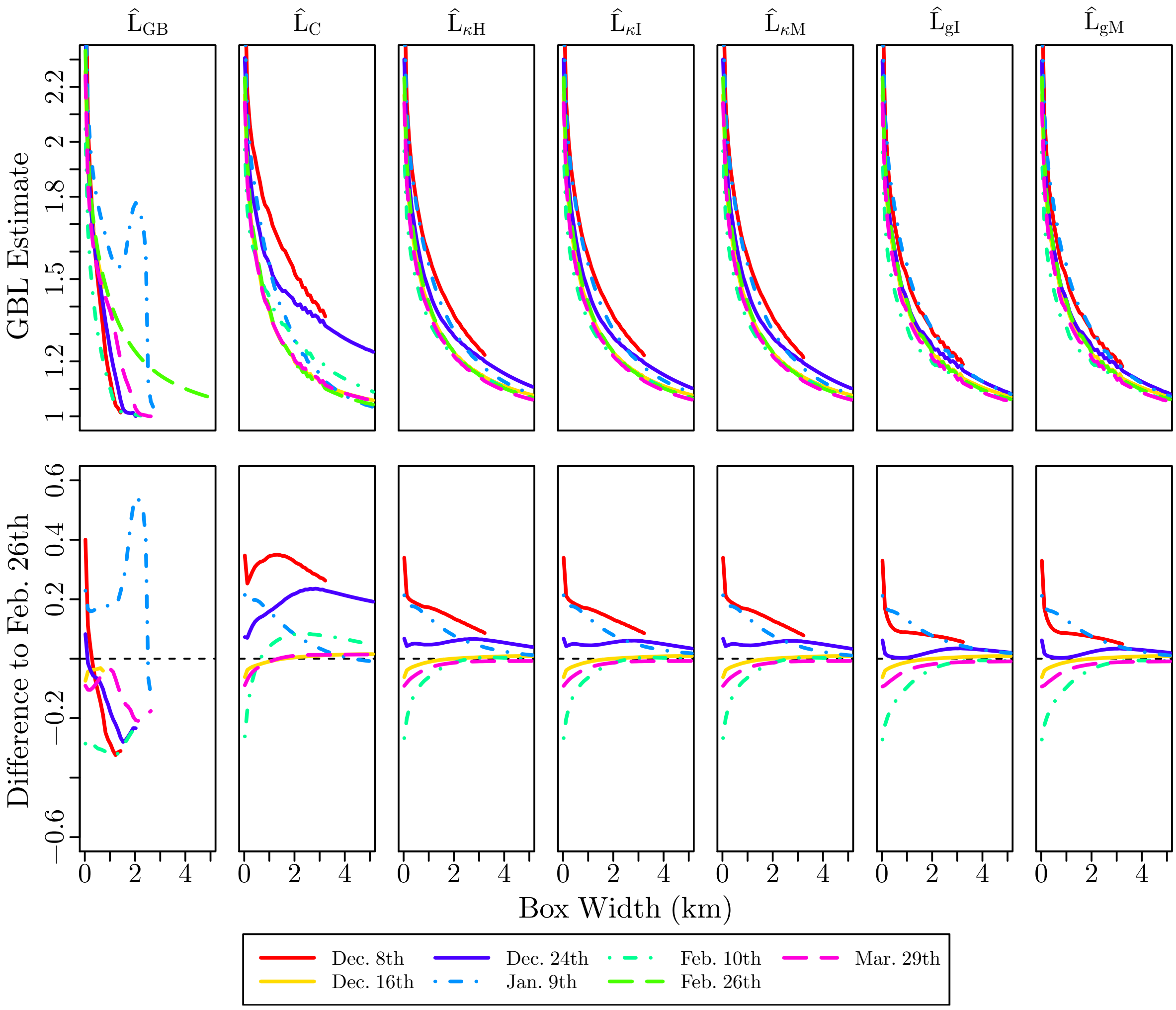

Figure 6: Results from each GBL estimator applied to the forest maps in Figure 5. *Top:* GBL estimates given square boxes. *Bottom:* The differences between estimates from the February 26 scene and estimates from the other scenes.

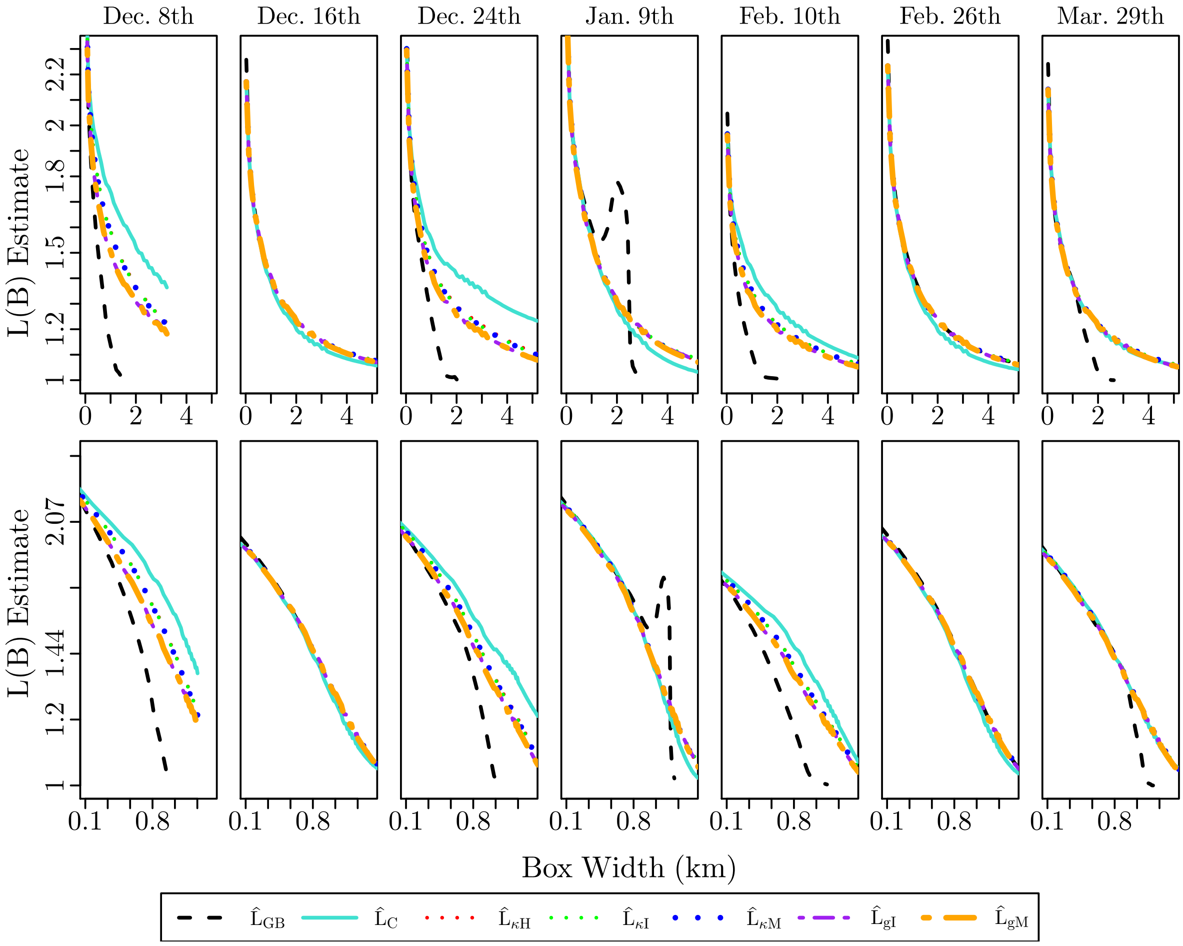

Figure 7: GBL estimates from each map in Figure 5 given square boxes. *Top:* Linear axes. *Bottom:* Log-log axes.

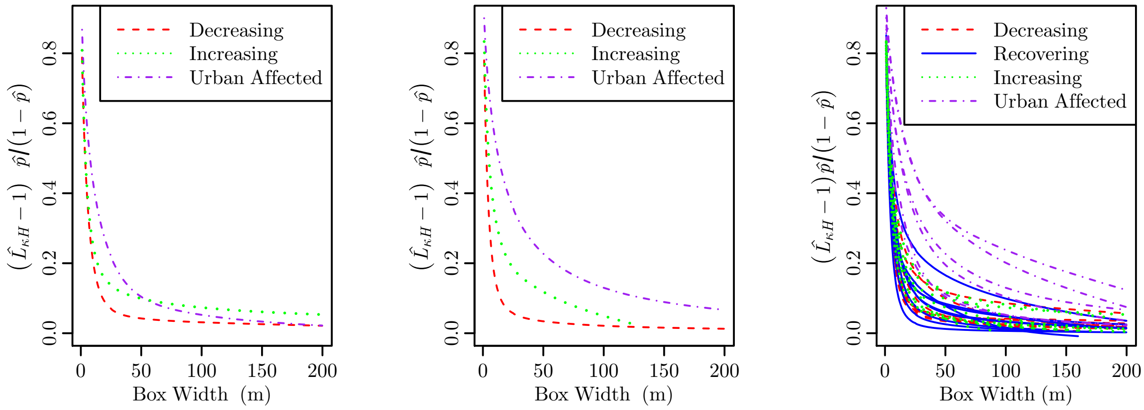

Figure 8: Standardised GBL estimates of disturbed forest parcels using $\widehat{\mathrm{L}}_{\kappa H}$. Left: The example parcels in Figure 9 observed to have between 37% and 40% tree canopy. Centre: The example parcels in Figure 9 observed to have between 65% and 67% tree canopy. Right: Estimates of GBL for all 33 parcels.

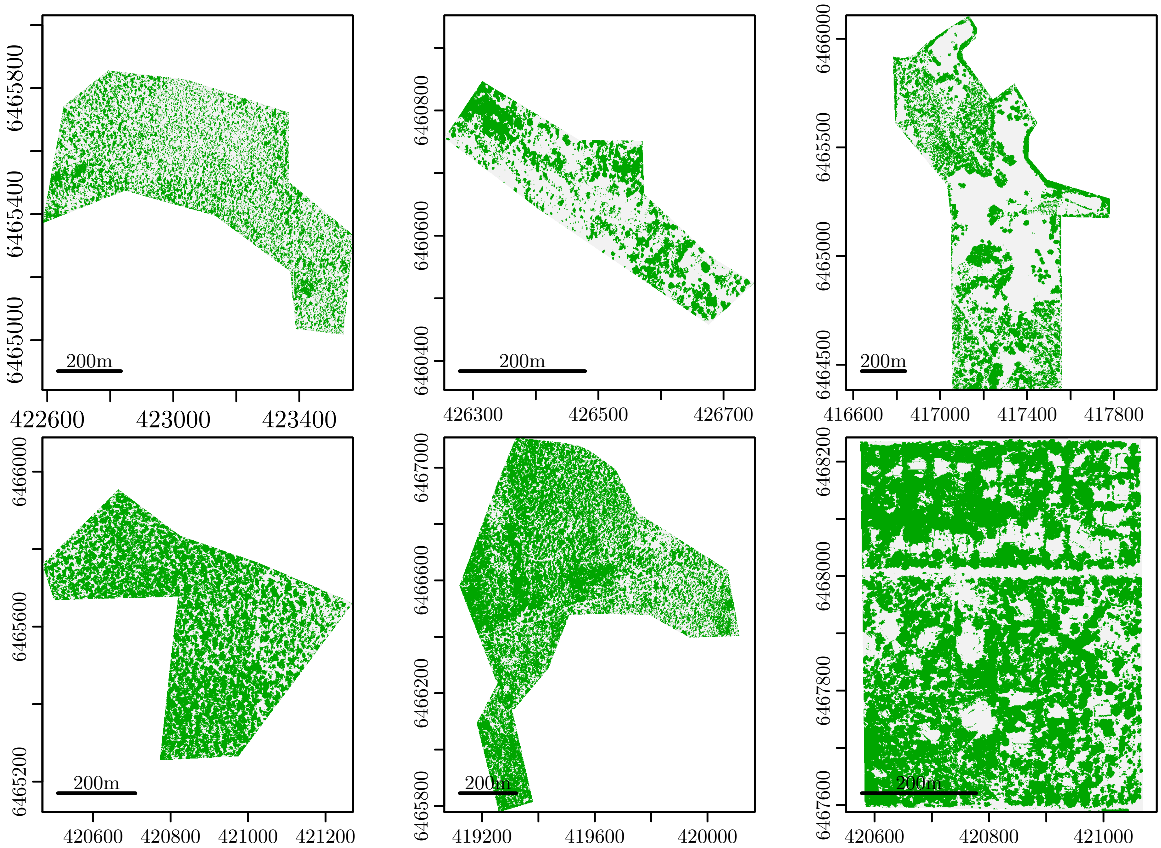

Figure 9: Forest Disturbance at Local Scales. Top: Parcels that are between 37% and 40% tree canopy. Bottom: Parcels that are between 65% and 67% tree canopy. From left to right: Parcels annotated as decreasing in cover, increasing in cover or subject to tree removal for urban development.

List of Tables

$\widehat{\mathrm{L}}_{\mathrm{GB}}$	$\widehat{\mathrm{L}}_{C}$	$\widehat{\mathrm{L}}_{\kappa H}$	$\widehat{\mathrm{L}}_{\kappa I}$	$\widehat{\mathrm{L}}_{\kappa M}$	$\widehat{\mathrm{L}}_{gI}$	$\widehat{\mathrm{L}}_{gM}$
78.93	26.00	16.30	16.31	16.28	17.14	17.11

Table 1: Average of the integrated squared discrepancy (ISD) of the GBL estimates relative to estimates from the February 26th map and excluding estimates from the December 8th and December 16th maps.